IEEE Access
Multidisciplinary | Rapid Review | Open Access Journal

Received July 11, 2017, accepted August 17, 2017, date of publication August 30, 2017, date of current version September 27, 2017.

Digital Object Identifier 10.1109/ACCESS.2017.2747398

Generalization of the Passivity Criterion for One-Port Devices Presenting Negative Real Part Admittances

ROBERTO BATISTA SARDENBERG[1,2] AND JOSÉ M. A. FIGUEIREDO[1]
[1]Physics Department, Universidade Federal de Minas Gerais, Belo Horizonte 30.161-970, Brazil
[2]Faculdade de Engenharia de Minas Gerais, Rua Aquiles Lobo, 524, Belo Horizonte 30.150-160, Brazil

Corresponding author: José M. A. Figueiredo (josef@fisica.ufmg.br)

This work was supported by part by the NTC/INCT Project and in part by the Brazilian Agencies CNPq and FAPEMIG.

ABSTRACT The physical validation of devices must comply with the principles of causality, passivity, and stability. For linear and time-invariant devices, it can be proved that passivity implies a causal transfer function. In this sense, it is understood that causality is a consequence of the passivity condition. Moreover, if the real part of the admittance is non-negative, it can also be demonstrated that the device is passive. The main subject of this work is a novel class of one-port passive devices presenting negative real part admittances on certain frequency ranges. Thus, the equations expressing the passivity condition, as far defined, are not applicable and the causality condition must also be checked. A theoretical model able to explain this effect and a generalization of the passivity condition, which fully address the applicability of the passivity-causality theorem are provided. The experimental verification of a specific device having this property is also shown. In this way, we report the results of a practical realization of a resonant circuit having negative real part values and a tunable positive to negative real part transition. As a possible outcome, novel passive circuits, such as oscillators and phase modulators covering the full trigonometric circle may be constructed. We also discuss the causality condition, show that negative real part admittances are causal and provide a new causality test that is in full consistence with the Kramers–Kronig relations.

INDEX TERMS Admittance measurements, negative real part admittance, passive circuit components, passivity condition, causality.

I. INTRODUCTION

A linear time-invariant device may be generally defined as a thermodynamic system having specially designed material properties. Its response depends on the validity of the small signal approximation, supported by the local equilibrium condition. The challenge in discovering new constitutive relations or the development of new devices is supported on the establishment of physical criteria that validates that response. In this sense, three basic and independent requirements must be satisfied: causality, stability and passivity [1]. The fulfilment of these requirements guarantees that data obtained from a device are reliable. The passivity condition, first introduced by Raisbeck [2], bids that the overall energy delivered to a device must be non-negative. A still more restrictive condition requiring that the net energy delivered to the device at any instant must be non-negative was introduced by Meixner [3], Konig and Meixner [4] and Youla *et al.* [5]. As first demonstrated in [5], all linear and time invariant devices subjected to the more restrictive passivity condition are also causal. However, the discussion presented by Wohlers [6] shows that passivity and causality should be considered as independent axioms, once they represent physical principles that surmount the class of linear and time-invariant devices. As a direct consequence of the passivity condition, it can be proved that the real part of the admittance must be non-negative [6]–[7].

These demands impose constraints on the set of admissible transfer functions, and widespread as a consistency test for measured data. For instance, electrochemical impedance data is generally checked by verifying if its real and imaginary parts satisfy the Kramers-Kronig relations [8]–[11]. Other applications include mechanical tests of viscoelastic materials [12], the study of reflection of electromagnetic waves from a surface [13], obtaining optical constants of thin absorbing films [14], the study of propagation modes on waveguides [15], the conductivity of high-Tc

superconductors from optical data [16], the attenuation coefficients on acoustic systems [17] and multi-layered optical systems [7].

In this work we deeply discuss the conditions a linear device must present in order to satisfy the causality and passivity principles. A novel mathematical condition that tests linear devices for causality is presented as well as a formula for the associated transfer function. It makes no use of the extension of the impedance over the upper complex plane. As a result, the causality principle can be tested by the sole use of experimental data. In sequence, a theoretical model of a linear device presenting negative real part admittance is discussed. It is demonstrated by first principles that this system is causal and passive. Consequently, a generalization of the passivity criterion formulated by Raisbeck [2] and Youla *et al.* [5] is necessary in order to accommodate this new class of devices. After the introduction of this extended passivity criterion, an experimental realization of a device having this property and an application on a resonant circuit are also provided.

II. CHECKING FOR CAUSALITY ON LINEAR DEVICES

The time-dependent response of a stationary linear system is written as a convolution of the excitation $v(t)$ and system's transfer function h. The excitation is assumed to be a causal function, defined by the relation $v(t) = \Theta(t-a)\, v(t)$. Here Θ is the step function. Thus, the response is given by

$$i(t) = \int_{-\infty}^{\infty} h(t-u)\,\Theta(t-u)\, v(u)\, du \tag{1}$$

In the Fourier space, system's response $I(\omega)$ is given as the product of the admittance $Y(\omega)$ times the amplitude of the excitation $V(\omega)$, that is $Y(\omega) = I(\omega)\, V(\omega)^{-1}$. In this sense, the admittance is of the correct effect/cause relation. Given the time-dependent excitation is a real-valued function it follows that the admittance possesses parity symmetries; specifically its real part is an even function of the frequency and the imaginary part is odd. The stability condition demands the admittance to have no poles on the real frequency axis. Moreover, the system cannot respond to infinity frequencies, thus the admittance goes to zero in this case. The causality condition Eq. (1) and the Tichamatch theorem [18] constrains the real and imaginary parts of the admittance to form a Hilbert pair

$$\begin{aligned} Y_r(\omega) &= \frac{1}{\pi} P \int_{-\infty}^{\infty} \frac{Y_i(s)}{\omega - s} ds \\ Y_i(\omega) &= \frac{-1}{\pi} P \int_{-\infty}^{\infty} \frac{Y_r(s)}{\omega - s} ds \end{aligned} \tag{2}$$

The impedance Z is the reciprocal of the admittance. Thus, impedance functions must have no zeroes on the real axis, share the same parity properties with the admittance and go to infinity at infinity frequencies. It must have zeroes in the upper half plane and must have no zeroes in the lower plane. Moreover, it must be analytic in the upper plane, but not bounded at infinity complex frequencies. Once it is not bounded in the upper plane it is not subject to the Tichmatich theorem. Therefore, we can assert the admittance as the proper Fourier transform of a physical transfer function. It has been usual to test impedance data [8]–[12] with the use of the Kramers-Kronig relation. However, this is not a causality test but rather a mathematical approach to obtain, for instance, the imaginary part from the real part, measured on a limited spectral region.

We shall now provide an alternative to Eq. (2) for testing causality. From the definition given in Eq. (1), the transfer function is given by

$$h(\tau)\,\Theta(\tau) = \frac{1}{2\pi} \int_{-\infty}^{\infty} Y(\omega) \exp(i\omega\tau)\, d\omega \tag{3}$$

By use of the symmetry properties of the admittance, the imaginary part of this equation is always null whatever the value of τ. The causality condition expressed by the Θ function forces the result of the integral in this equation to vanish for negative τ values. The converse is also true. A null result of the real part configures a validation of the causality principle. This fact can be mathematically expressed as follows. The negative parameter τ is redefined as $-\tau$, $(\tau > 0)$. Then, a system is causal if and only if the following equation

$$Zero(\tau) \equiv \frac{1}{\pi} \int_{0}^{\infty} [Y_r(\omega)\cos(\omega\tau) + Y_i(\omega)\sin(\omega\tau)]\, d\omega \tag{4}$$

is null for $\tau > 0$. Consequently, Eq. (4) can be considered as a causality test. It is a simpler recipe for testing causality when compared to the Krammers-Kronig (KK) relations given that numerical computation of KK demands a regularization procedure (poles removal). Once the check for causality is successful, the condition expressed in Eq. (4) can be reinserted on Eq. (3), now calculated for positive τ values. The result is an expression for the transfer function, written as the spectral integration of the admittance, without the need of the use of complex frequencies, and given by

$$h(\tau) = \frac{2}{\pi} \int_{0}^{\infty} Y_r(\omega)\cos(\omega\tau)\, d\omega \tag{5}$$

If an analytic expression valid in the upper complex plane and consistent with a given set of impedance data is available, the transfer function can be computed as

$$h(\tau) = i \sum_{zeroes} \frac{\exp(i\omega\tau)}{Z(\omega)} \tag{6}$$

Below, we present the result of Eq. (4), (5) and (6) for the admittance derived from the forced Drude model:

$$m\ddot{x} + kx + \alpha\dot{x} = F_0 \exp(i\omega t)$$

and given by: $Y(\omega) = \left[R + i\omega L + (i\omega C)^{-1}\right]^{-1}$. The lumped circuit parameters R, L and C are written in terms of the Drude parameters, carrier concentration and sample geometry. This model gets in full compliance with the theory developed here. The validation of this admittance with the use of equations (4)-(6) is presented in Fig. 1 for a sample series RLC circuit with the following parameters $R = 50\Omega$, $L = 10\mu H$ and $C = 0.1nF$. Observe that the calculated Zero function values are in fact much smaller than the transfer function values. Besides, the transfer function retrieves the same values regardless of whether it is calculated by Eq. (5) or Eq. (6). As a result we have demonstrated that Eq. (4) and (5) can be used as a practical causality test.

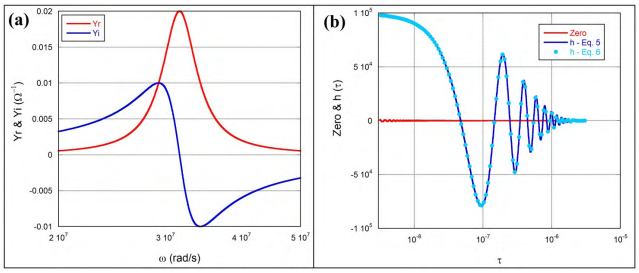

FIGURE 1. Sample RLC circuit. (a) Admittance spectrum. (b) Zero function and transfer function calculated by means of Equation (5) (dark blue line) and by means of Equation (6) (light blue symbols).

III. MECHANICAL MODEL OF A NEGATIVE REAL PART ADMITTANCE DEVICE

Now we present a theoretical model of a mechanical one port linear system having negative real part admittance. By introducing this mechanical analogy we expect to better clarify and present the negative real part effects as an admissible physical condition for a specific class of linear and passive devices. As shown below, this effect demands that some portion of the device's volume must be sensitive to the externally applied force field. An actual electrical device presenting the effect is introduced later in this article.

The model consists solely of particles and springs without any internal energy source. Hence, there is no reason to suppose it is an active system. The way an external excitation interacts with the system is crucial in determining the character of its admittance. If the energy source provides a force field which extends itself over the device's volume, an interval of frequencies exists such that the admittance attains negative real part values. Given the equivalence of the passivity criterion and the non-negative character of the real part admittance, this device cannot be considered as passive, at least as formerly presented on [5]. Interestingly, even under this condition the imaginary and real parts of its admittance form a Hilbert pair, which assures that the device's response is causal. In order to solve these apparent inconsistencies, an extension of the passivity criterion that considers the energy delivered and stored over the device's volume is discussed. Based on this new definition we shall prove that passiveness is restored and, given the causal character which is also shown to be valid for this device, the passivity-causality theorem is fully preserved.

Firstly, consider a system composed of N particle-spring pairs forming a linear chain and subjected to an external energy source. The N = 2 case will be deeply discussed and its drawings are presented in Fig. 2.

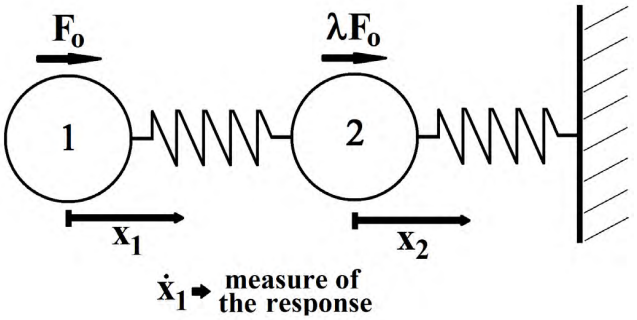

FIGURE 2. Schematics of the two particle-spring mechanical model (N = 2).

Two types of energy source are considered. In one situation both particles are subjected to the force ($\lambda = 1$; force field). In the other situation only the first particle is excited ($\lambda = 0$; localized excitation).

It is worth noting that a potential difference is established between the first mass and the last spring, which is fixed to a rigid wall that is considered to be the system's ground. The particles are driven in only one direction (see Fig. 2 and 5). Therefore we have fields and currents in only one direction, all similar to the simplest case of a resistor subject to a potential difference. Energy is simultaneously delivered to all parts in the device. But the current is measured at the geometrical device's entrance – one of the two terminals – which corrensponds to the first mass in our model. This analogy is particularly useful for the large N case. All of these facts and definitions suffice to classify this system as a one port device. Yet, energy balance concerns the whole device's volume and is correctly considered in our model in Section IV. On contrast, multiple port case demands fields and currents in many directions (see for instance Fig. 4.4 and 4.5 of Pozar's book [19]). In fact, as pointed out by Oliner [20], Wheeler coined the term port as generalization and more precise definition of the two-terminal pair concept.

The springs are massless, and both particles are subjected to viscous damping. The force field case may be accomplished by charging both particles and subjecting them to an applied homogeneous electric field. The localized excitation may be achieved by charging just the first particle. Thus, as indicated in Fig. 2, the system's port refers to the terminals on the particle 1 and on the wall (system's ground). Dynamical equations for this system read

$$\begin{aligned} m\ddot{x}_1 + k\,(x_1 - x_2) + m\alpha\dot{x}_1 &= F_0 \exp(i\omega t) \\ m\ddot{x}_2 + k\,(2x_2 - x_1) + m\alpha\dot{x}_2 &= \lambda F_0 \exp(i\omega t) \end{aligned} \qquad (7)$$

Although the source force field extends itself over the system's volume, the response is defined by the first particle movement, which is proportional to the reading of a current meter placed in series to it. With this definition device admittance Y is, unless by a constant, equal to particle 1 velocity amplitude. The resulting admittances for both excitation cases $\lambda = 1$ and $\lambda = 0$ are given by

$$\begin{aligned} Y\underset{\lambda=1}{(\omega)} &= \frac{i\omega}{m}\frac{3\omega_o^2 - \omega^2 + i\omega\alpha}{\left[\omega_o^2 - \omega^2 + i\omega\alpha\right]\left[2\omega_o^2 - \omega^2 + i\omega\alpha\right] - \omega_o^4} \\ Y\underset{\lambda=0}{(\omega)} &= \frac{i\omega}{m}\frac{2\omega_o^2 - \omega^2 + i\omega\alpha}{\left[\omega_o^2 - \omega^2 + i\omega\alpha\right]\left[2\omega_o^2 - \omega^2 + i\omega\alpha\right] - \omega_o^4} \end{aligned} \quad (8)$$

Figure 3 displays the admittance spectrum, in the $0.4 \leq \omega \leq 2.4$ interval, which was calculated by the use of Eq. (8), for $\omega_o \equiv \sqrt{k/m} = 1$, $m = 1$ and $\alpha = 0.1$. Notice that the admittance presents a negative real part peak for the force filed case. So far, it has been believed that any passive device must present non-negative real part admittance. The occurrence of a negative real part has been associated to active energy sources inside device's volume. In the present model the velocity of particle 1 is opposite to the applied force inside a specific spectral region and this is the cause of the negative real part admittance. We have checked that the velocity of particle 2 is always in-phase with the force. Besides, this complex valued data was checked for causality with the use of Eq. (2). For every calculated point ω, the lower infinite limit on the integrals was substituted for -50ω and the upper limit for 50ω. As can be seen in Fig. 3, this procedure allowed good enough convergence for affirming this model as causal, that is, the real and imaginary parts do form a Hilbert pair on both excitation cases.

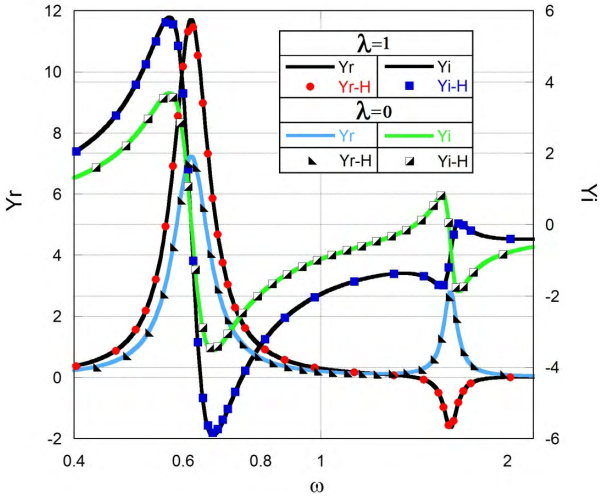

FIGURE 3. Schematics of the two particle-spring mechanical model (N = 2).

The alternative causality condition introduced here (Eq. (4)) and the transfer function defined by Eq. (5), were also checked for the field excitation case, as can be seen in Fig. 4.

The calculated values of the Zero function are small in comparison to the transfer function values for every

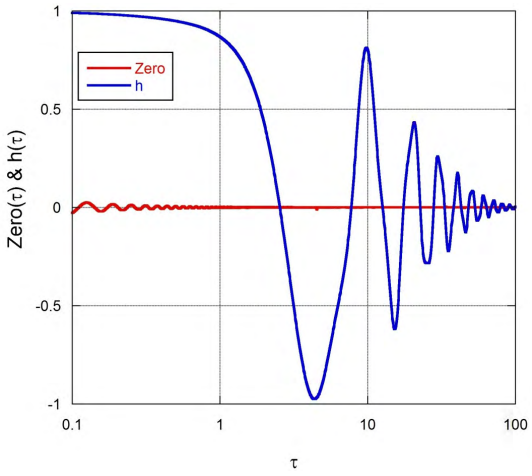

FIGURE 4. Zero function and transfer function of the mechanical model (N = 2).

frequency. This fact is another support for the validation of the negative real part admittances as consistent with causal responses.

Results for the N = 4 case shall be presented in a summarized way. Schematic is provided in Fig. 5 below

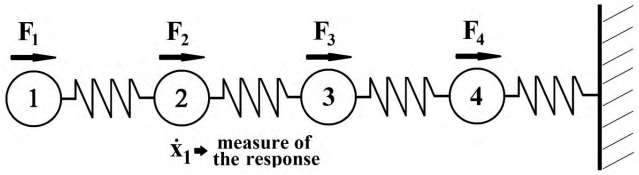

FIGURE 5. Schematics of the four particle-spring mechanical model (N = 4).

In the localized excitation setup the generator applies a force only to particle 1 ($F_1 = 1; F_2 = F_3 = F_4 = 0$). In the force field case, all particles are subjected to a force produced by the source. We present here the results for some force profiles. The case of a uniform profile ($F_1 = F_2 = F_3 = F_4 = 1$) is presented in Fig. 6 along with results for the localized excitation setup. In all situations we have checked that the causality principle is satisfied, through the use of the KK relations and the Zero function.

As expected, four resonant peaks are present in both cases. Two negative real part peaks are present for the force field excitation. The localized excitation case has positive real part admittance for all finite frequency values and presents a spectrum that resembles conventional devices. Figure 7 displays results for various exponential profiles in which particle n is excited by a force equal to $F(n) = \exp(-q(n-1))$, having different decay constants. Part (a) presents a broad real part admittance spectrum while parts (b) and (c) picture closer visualizations of the peaks. More homogenous field distributions (small decay constants) provide deeper negative real part peaks. A transition from a conventional device (no negative peaks) to an "exotic" one (a negative peak is present) is observed for a decay constant $q \approx 0.28$.

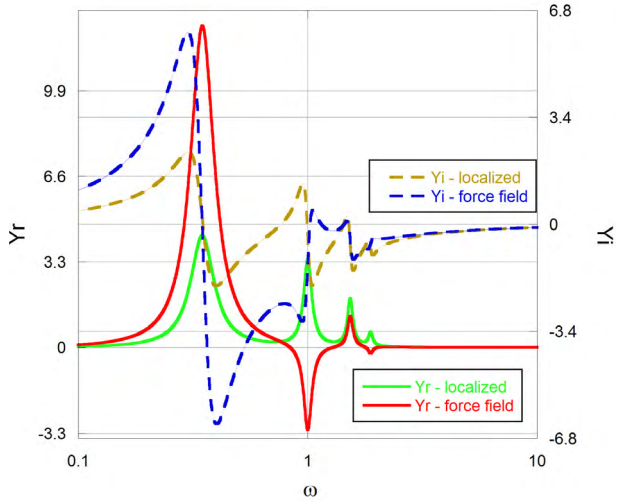

FIGURE 6. Admittance spectrum of the mechanical model (N = 4) for both the localized excitation and force field setups. Solid lines represent the real part while dashed lines represent the imaginary part.

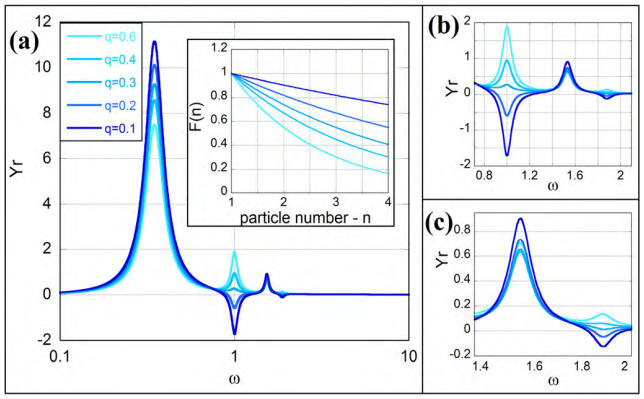

FIGURE 7. Real part admittance spectrum of the mechanical model (N = 4) for exponential force field profiles with several decay constants. (a) Broad spectrum and force field profile. (b) and (c) Closer visualizations to the high frequency real part peaks.

IV. GENERALIZATION OF THE PASSIVITY CRITERION

The passivity condition, as initially proposed in [2] is written as $\int_{-\infty}^{\infty} i(t)\, v(t)\, dt \geq 0$. In this equation, the response $i(t)$ is caused by the excitation $v(t)$ and is measured at one of the device's terminals. For a linear, time-invariant system, this condition can be written in terms of the admittance and the Fourier transform of the excitation as $\int_{-\infty}^{\infty} Yr(\omega)\, |V(\omega)|^2\, d\omega \geq 0$, valid for an arbitrary excitation $V(\omega)$. Therefore the passivity condition demands that the real part admittance must be non-negative. Since the model presented here seems to be intrinsically passive and demonstrated to be causal, an improvement of the passivity criterion is demanded. Trustfully, what happens is that all particles get energy directly from the source. Then, for some frequencies, particle 1 returns part of its energy back. Once particle 1 velocity is defined as the system's response, this is the cause of the negative real part admittance. However, as shown below, total energy delivered to the device is positive at all times.

In [3] the passivity condition is written as $\int_{-\infty}^{t} i(u)\, v(u)\, dt \geq 0$. In the language of the model presented here it is written as the exigency that $\int_{-\infty}^{t} \dot{x}_1(u)\, F(u)\, dt \geq 0$. This calculation will be considered for the case N = 2. The real part of the admittance is non-negative for all frequencies in the localized excitation situation, so the passivity integral is automatically satisfied. In the force field situation, the passivity integral (calculated at the device's port) results in

$$0.5\left[m\dot{x}_1^2 + kx_1^2\right] + m\alpha \int_{-\infty}^{t} \dot{x}_1^2(u)\, du - k\int_{-\infty}^{t} \dot{x}_1(u)\, x_2(u)\, du$$

which has no defined signal. In both calculations we had assumed that the particles were motionless for negative infinite times. As expected, the passiveness failure we have obtained is consistent with the existence of negative real part data. On the other hand, by its own nature it is reasonable that such a simple system cannot be active. In order to encompass its presumed passiveness into a formal theory, a new definition formula is introduced. Total energy delivered by the source is given by:

$$E(t)_{\lambda=1} = \int_{-\infty}^{t} [\dot{x}_1(u) + \dot{x}_2(u)] F(u)\, du \tag{9}$$

The kinetic and the damping contributions are grouped and define the following non-negative quantities

$$E_1^*(t) = \frac{m}{2}\dot{x}_1^2 + m\alpha \int_{-\infty}^{t} \dot{x}_1^2(u)\, du \geq 0$$

$$E_2^*(t) = \frac{m}{2}\dot{x}_2^2 + m\alpha \int_{-\infty}^{t} \dot{x}_2^2(u)\, du \geq 0$$

Equation (9) is then rewritten as:

$$E(t)_{\lambda=1} = E_1^* + E_2^* + \frac{k}{2}x_1^2 + kx_2^2 - kx_1x_2$$

It can be proved that this quadratic form has only one minimum located at the point $x_1 = x_2 = 0$ and at this point, the energy delivered is given by

$$E_{\lambda=1}(x_1 = x_2 = 0) = E_1^* + E_2^* \geq 0$$

As a result, this device can be considered to be passive, despite its negative real part admittance. The passivity integral shall be modified in order to accommodate the energy distribution over the device's volume. That is, the standard one port passivity test accounts only for the energy delivered directly through the port.

Generally, supposing that for a specific device the concept of a linear passive and time-invariant response can be locally defined inside the device's volume. A class of such system is presented in [21] and [22]. Moreover, we also suppose that in these extended systems the excitation is a force field $\vec{F}(\vec{r}, t)$ that interacts with different portions of the sample and produces a space-dependent response $\vec{j}$. The passivity test appropriated to this case is then rewritten as

$$\int_{-\infty}^{t} \left[\int_V \vec{F}(\vec{r}, u) \cdot \vec{j}(\vec{r}, u) d^3\vec{r}\right] du \geq 0 \tag{10}$$

which is a generalization of Eq. (9). The local property defines, in turn, a local response function similar to a locally-defined admittance, yet inaccessible to outside measurements (otherwise it becomes a new device port). The passivity condition for $t \to \infty$ is now written as

$$\int_V d^3\vec{r} \int_{-\infty}^{\infty} Yr\,(\vec{r},\omega)\,\vec{F}\,(\vec{r},\omega)\cdot\vec{F}^{*}\,(\vec{r},\omega)\,dt \geq 0$$

and, in this perspective, device's admittance may assume negative real part values, despite the positive energy outflow from the source. In Eq. (10), the superior limit can be extended to infinity by mathematically forcing the excitation field to vanish for $u > t$ [6]. This procedure gives a universal validation for passive systems presenting negative real part admittances with the use of Eq. (10).

V. AN EXPERIMENTAL REALIZATION OF A NEGATIVE REAL PART ADMITTANCE PASSIVE DEVICE

An experimental accomplishment of a device presenting negative real part admittance can be observed in the radio frequency region. We have discovered that a coil possessing low inter-spire capacitance and a wire length of the same order of the wavelength of the applied potential is a candidate for presenting negative real part effects. At low frequencies this kind of coil presents the standard inductance characteristics. At higher ones the real part admittance enters in the negative real part spectral region. A minimum value is attained at still larger frequencies (an inverted peak) and the polar angle crosses the $[\pi,-\pi]$ topological line. Here we show this effect for an aluminum coil having a wire length of 12.5m, a wire diameter of 0.2mm, a spire spacing of 2.6mm and a coil diameter of 40mm in Fig. 8.

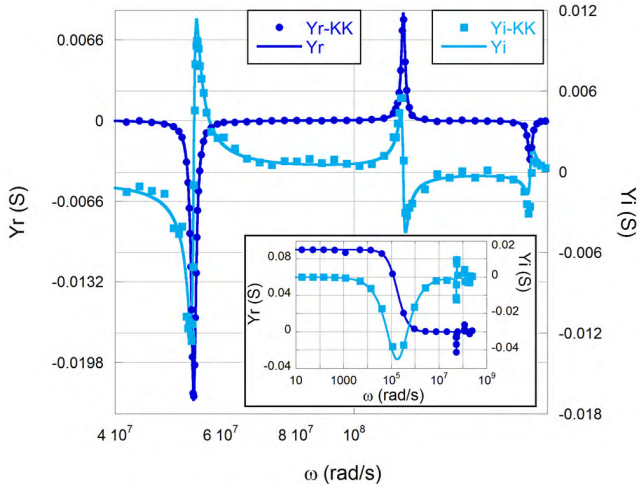

FIGURE 8. Admittance spectrum of the aluminum coil. Solid dark line: measured real part. Solid light line: measured imaginary part. Symbols: Admittance calculations by means of the Kramers-Kronig relations derived from Eq. (2).

Measurements were performed with a Novocontrol Alpha-A impedance meter [23], in a shielded room [24]. The coil was placed inside an aluminum box having 5mm thick walls in order to completely exclude possible external interferences. Also, admittance data were checked for linearity in the potential range from 10mV to 2000mV. The calculated real and imaginary parts using the Krammers-Kronig equations derived from Eq. (2) are also presented in Fig. 8. The Zero function and the associated transfer function values for this coil are presented in Fig. 9.

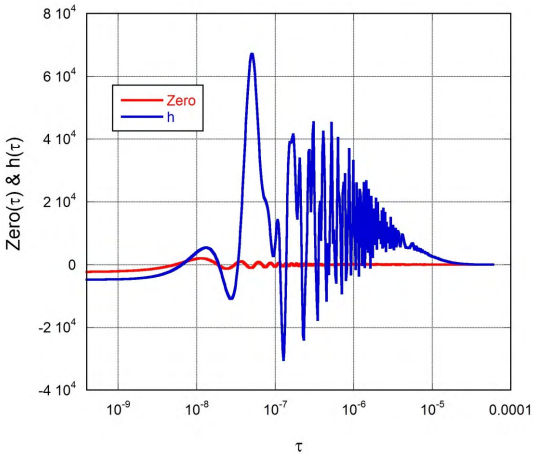

FIGURE 9. Zero function and transfer function for the aluminum coil.

Despite the rich spectral structure of this device, the obtained Zero values are still reasonably smaller than those of the transfer function.

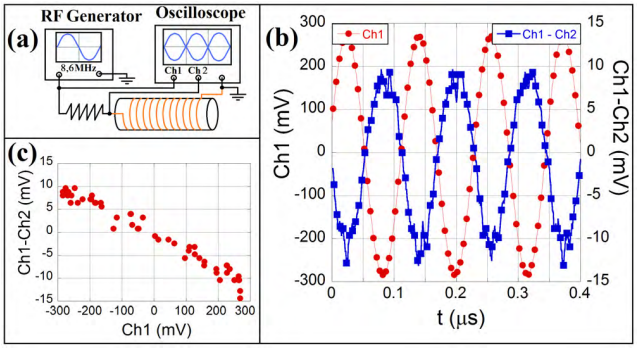

FIGURE 10. Oscilloscope measurements. (a) Schematics of the circuit. (b) Generator (circles) and shunt voltage (squares). (c) Lissajous pattern. Vertical: shunt voltage (Ch1-Ch2). Horizontal: generator voltage (Ch1).

As a more direct view of the negative real part effect, this coil and an in-series 2.4Ω shunt resistor were plugged into a RF generator (Rohde & Schwarz-SMY01). Fig. 10(a) shows the schematics of this circuit. It is worth noting that in this configuration the shunt resistor is used as a current sensing element. Oscilloscope Channel 1 monitors the generator's output whereas Channel 2 monitors the coil voltage. The input current in the coil is approximately given by the Channels' voltage difference divided by the shunt resistance value. In Fig. 10(b) we present the time dependence of the difference Ch1-Ch2 and Ch1 data at the frequency of 8,6MHz. A clear anti-phase pattern is present. The Fig. 10(c) shows the

Lissajous pattern associated with data presented in Fig. 10(b). The left-inclined Lissajous pattern configures the negative real part effect. Although causality is assured for this device, we did not directly prove its passiveness. However, the care taken in performing the measurements as well as its own basic conception support a claim for passivity. Moreover, it is clear that the reasoning concerning the mechanical model presented here strongly sustains that claim.

In light of possible applications, it would be desirable to test the effect at higher frequencies. Obviously, for the VHF range and above additional care must be taken on device building, such as avoiding parasitic impedances. Here we report an experiment of the type shown in Fig. 10, this time using a spire instead a coil. For this goal, our RF signal generator and a 500 MHz HP-54610B oscilloscope were used. The 2.4Ω shunt resistor was plugged in series to a single circular copper spire having 50mm diameter, here used as the device. A picture of this montage is presented in Fig. 11.

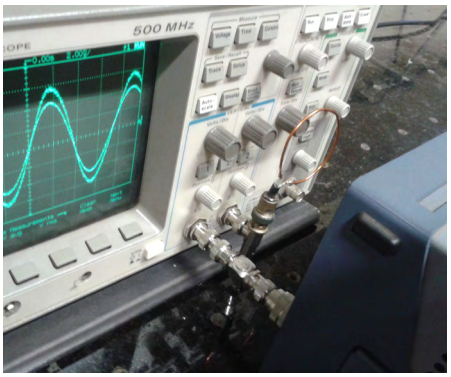

FIGURE 11. Picture of the set up for the 50mm copper spire measurements.

Data were collected by use of a computer having a GPIB interface. Measurements were performed in the range 10 – 320 MHz and Lissajour plots for a selected set of excitation frequencies are presented in Fig. 12 (a). In Fig. 12 (b), oscilloscope scan data, similar to those of Fig. 10 (b), are shown for the frequency of 124MHz.

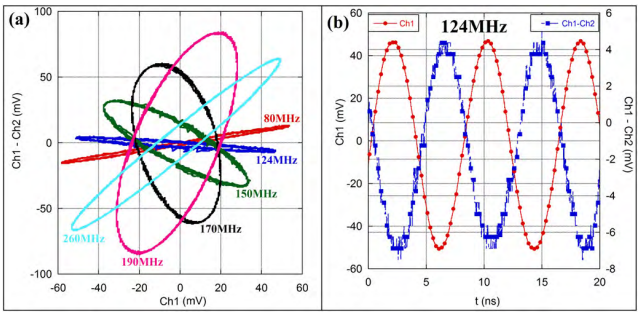

FIGURE 12. Copper spire oscilloscope measurements data. (a) Lissajous pattern for a selected set of excitation frequencies. (b) Oscilloscope readings at the frequency of 124MHz.

Our Lissajour data show, for the first time, the major axis of the ellipsis covering four quadrants of the phase space. Oscilloscope input impedance and spurious capacitances in the signal lines prevented observation of the effect at still higher frequencies in our experimental setup, even with the use of smaller spire radius. Nevertheless it seems clear that negative real part admittances effects are also verified in the VHF range thus promising their use on the conception of new RF circuits and applications. Although advanced technical challenges may rise, its use in the microwave range sounds possible as well.

VI. MATERIAL EFFECTS IN THE RF RANGE

In order to test, at least qualitatively, how different materials affect the negative resonant peak of the real part admittance, additional measurements were performed on various types of coils in the RF range, this time performed on our laboratory workbench without any shielding. As before, the Novocontrol equipment has been used on all spectra measurements. Several winding wire materials were used and all data we collected undoubtedly confirm the existence of the negative real part effects. Four different coils having 40 mm diameter, a wire length of 12.6m and a spire spacing of 2.5mm were constructed. Wires of constantan, brass, aluminum and copper were used; and diameter varied among the materials. In this way, admittance data were normalized to the aluminum wire diameter. We present in Table 1 a list of the materials used, their respective wire diameters, the area scaling normalization factor and material conductivities.

TABLE 1. Wire materials, diameters and conductivities.

Material	Diameter φ(mm)	Normalization factor $\xi=(\varphi_{Al}/\varphi)^2$	Conductivity σ (10^6S/m)
Cu	0.11	3.25	59.6
Al	0.20	1	35.5
Brass	0.45	0.20	15.6
Const.	0.10	4	2.0

In Table 2 we present the admittance measured at the frequency of 10Hz (the wire conductance G), the ratio of conductivities also choosing aluminum as a reference and also the respective ratio of measured conductance.

TABLE 2. Conductivities and conductance ratios.

Material	Normalized Conductance (ξ G)	Conductivity ratios σ/ σ_{Al}	Normalized conductance ratios ξ G/G_{Al}
Cu	0.1953	1.676	1.664
Al	0.0935	1	1
Brass	0.0377	0.439	0.403
Const.	0.0051	0.056	0.055

Non-normalized admittance data are presented in Fig. 13 for all coils whereas normalized data are presented in Fig. 14. This figure also shows detailed high frequency data displaying the negative peak resonances.

We also checked for linearity on all measurements. As an example of these results, Fig. 15 presents admittance data of

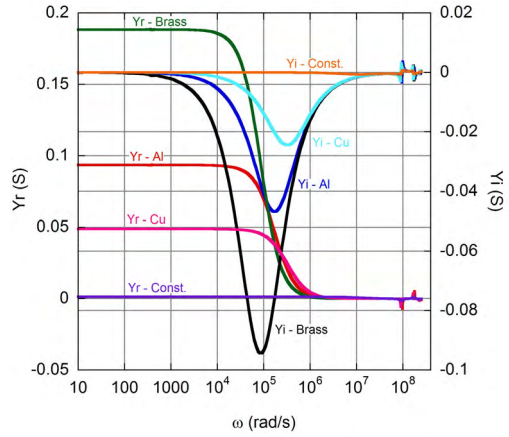

FIGURE 13. Non-normalized admittance data for all coils.

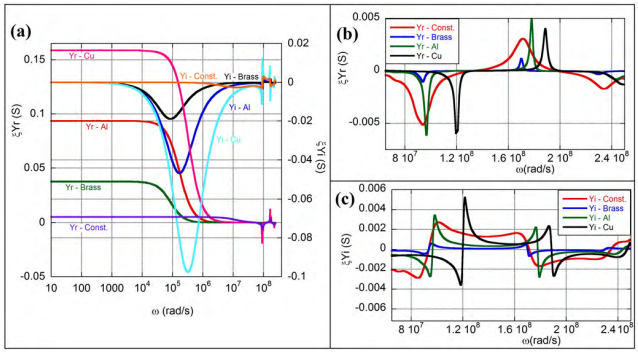

FIGURE 14. Normalized admittance data for all coils. (a) Broad spectral data. (b) Close visualization at high frequencies for the real part. (c) Close visualization at high frequencies for the imaginary part.

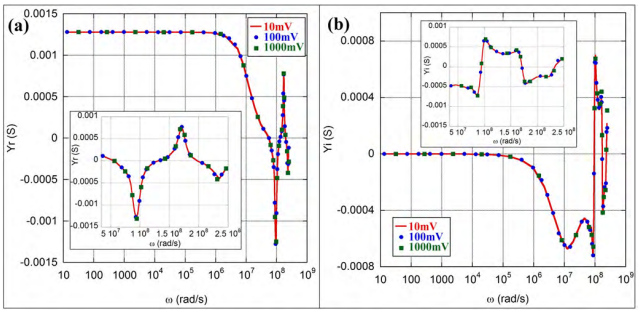

FIGURE 15. Admittance measurements of the constantan coil from 10 to 1000mV. (a) Real part and (b) Imaginary part.

the constantan coil measured in the range 10 to 1000 mV. Notice that, for better visualization purposes, a slightly different set of frequency values for each curve was chosen for this picture. All other coils presented similar results.

A first sight of the high frequency spectral region of all coils, as presented in Fig. 14(b), 14(c) and 15, is their similarity to Fig. 6 and 7, which present the admittance for the N = 4 linear chain model. Specifically, both sets of data present three real part peaks and, two of them are negative. In both cases the negative-positive-negative order is followed.

The normalized real part spectra of all coils present in the low frequency region the expected sequence of increasing values based on the material conductivity. We show in the last columns of Table 2 the normalized conductivity ratios for each material, in reference to the aluminum case, as well as the measured and normalized real part admittance ratios at the frequency of 10 Hz. As expected, this set of data is self-consistent. Major deviance occurs for the Brass case because the composition of this alloy may vary substantially on the available commercial products.

The high frequency spectral region for all coils, locus of the negative real part effects, is shown in Fig. 14(b) and 14(c). The larger peak width for the constantan case is notable. This effect may be related to its greater loss. Using the same reasoning, the most conductive of the used materials – copper – presents the deepest negative peak. Line widths of copper and aluminum negative peaks are comparable. Remarkably, this high frequency spectrum of the brass coil is almost absent.

It seems evident from our data that material properties are present and also relevant in determining the high frequency spectral region admittance. Even though there are still minor constructive differences on our coils, the observed material effects are relevant enough to consider their use on the conception of novel devices.

VII. APPLICATION CIRCUIT

The possibility of negative real part admittances opens a window for a new circuit type, able to cover the full trigonometric circle of the phase angle. In order to explore this effect, we have mounted our coil in parallel to an air filled variable spacing capacitor, made of two 25mm diameter stainless steel plates, supported on a one micrometer resolution displacer. The real part spectrum of the impedance at various plate separations is presented in Fig. 16.

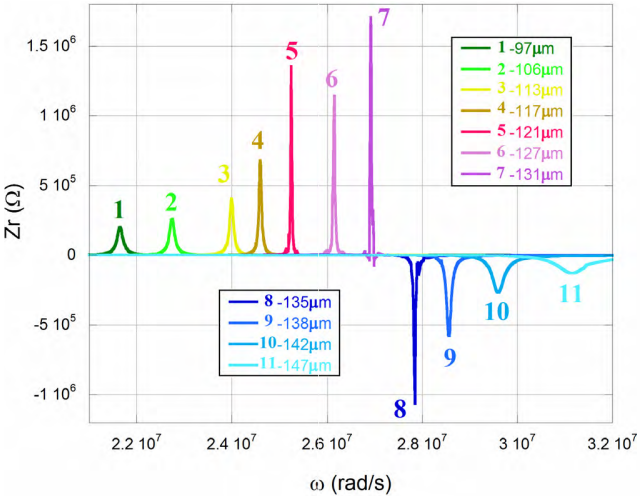

FIGURE 16. The real part impedance spectrum of the resonant circuit for several plate separations.

A flip of the real part resonant peak is observed for a specific plate separation. This plate spacing is critical in the sense that small changes on it lead to a change in the sign of

the real part peak. This kind of circuit may become valuable in the engineering of a new class of passive phase modulators able to surmount the so far limited $[-\pi/2, \pi/2]$ phase angle interval spanned by standard passive devices.

VIII. CONCLUSIONS

A one port passive linear and time-invariant device may present negative real part admittance and still be in full consistence with the causality principle. This effect occurs for those devices whose physical properties allow an extended energy delivery throughout its volume. We proposed a new passivity condition that conforms the distributed (force field) excitation mode. It seems that a homogeneous force field produces deeper negative real part peaks. It is expected that new devices would be able to explore the broader phase angle interval favored by negative real part admittance effects.

Concerning the data from the coils we have built, evidence was found supporting the existence of material effects in the high frequency region of the admittance spectrum. This way, it seems clear that the novel admittance effects presented in this work are sensitive to material properties.

We also showed that negative real part admittances can be tuned on resonant circuits. A possible consequence is the construction of novel phase modulator circuits able to simultaneously process two communication channels, a conventional one having the $[-\pi/2, \pi/2]$ interval, and an ''exotic'' one having the $[\pi/2, 3\pi/2]$ interval.

ACKNOWLEDGMENT

The authors are grateful to Eng. Arnaud Colin of Fiat-Chrysler Automobile/ LATAM (Betim-MG-Brazil) for making the shielded room facility available.

REFERENCES

[1] P. Triverio, S. Grivet-Talocia, M. S. Nakhla, F. G. Canavero, and R. Achar, ''Stability, causality, and passivity in electrical interconnect models,'' *IEEE Trans. Adv. Packag.*, vol. 30, no. 4, pp. 795–808, Nov. 2007.

[2] G. Raisbeck, ''A definition of passive linear networks in terms of time and energy,'' *J. Appl. Phys.*, vol. 25, no. 12, pp. 1510–1514, Dec. 1954.

[3] J. Meixner, ''Thermodynamische erweiterung der nachwirkungstheorie,'' *Zeitschrift Phys.*, vol. 139, no. 1, pp. 30–43, Feb. 1954.

[4] H. König and J. Meixner, ''Lineare Systeme und lineare transformationen. Dem gedenken an hermann ludwig schmid gewidmet,'' *Math. Nachrichten*, vol. 19, nos. 1–6, pp. 265–322, Dec. 1958.

[5] D. Youla, L. Castriota, and H. Carlin, ''Bounded real scattering matrices and the foundations of linear passive network theory,'' *IRE Trans. Circuit Theory*, vol. 6, no. 1, pp. 102–124, Mar. 1959.

[6] M. R. Wohlers, *Lumped and Distributed Passive Networks: A Generalized and Advanced Viewpoint*, H. G. Booker and N. DeClaris, Eds. New York, NY, USA: Academic, 1969, pp. 29–32, ch. 2. [Online]. Available: http://elsevier.com/books

[7] Y. Liu, S. Guenneau, and B. Gralak, ''Causality and passivity properties of effective parameters of electromagnetic multilayered structures,'' *Phys. Rev. B, Condens. Matter*, vol. 88, p. 165104, Oct. 2013.

[8] D. D. Macdonald and M. Urquidi-Macdonald, ''Application of Kramers–Kronig transforms in the analysis of electrochemical systems I. Polarization resistance,'' *J. Electrochem. Soc.*, vol. 132, no. 10, pp. 2316–2319, Jun. 1985.

[9] M. Urquidi-Macdonald, S. Real, and D. D. Macdonald, ''Application of Kramers–Kronig transforms in the analysis of electrochemical impedance data II. Transformations in the complex plane,'' *J. Electrochem. Soc.*, vol. 133, no. 10, pp. 2018–2024, Oct. 1986.

[10] J. M. Esteban and M. E. Orazem, ''On the application of the Kramers–Kronig relations to evaluate the consistency of electrochemical impedance data,'' *J. Electrochem. Soc.*, vol. 138, no. 1, pp. 67–76, Jan. 1991.

[11] B. A. Boukamp, ''Practical application of the Kramers–Kronig transformation on impedance measurements in solid state electrochemistry,'' *Solid State Ionics*, vol. 62, pp. 131–141, Jul. 1993.

[12] L. Rouleau, J.-F. Deü, A. Legay, and F. Le Lay, ''Application of Kramers–Kronig relations to time–temperature superposition for viscoelastic materials,'' *Mech. Mater.*, vol. 65, pp. 65–75, Oct. 2013.

[13] S. A. R. Horsley, M. Artoni, and G. C. L. Rocca, ''Spatial Kramers–Kronig relations and the reflection of waves,'' *Nature Photon.*, vol. 9, pp. 436–439, Jun. 2015.

[14] R. Nitsche and T. Fritz, ''Determination of model-free Kramers–Kronig consistent optical constants of thin absorbing films from just one spectral measurement: Application to organic semiconductors,'' *Phys. Rev. B, Condens. Matter*, vol. 70, p. 195432, Nov. 2004.

[15] M. W. Haakestad and J. Skaar, ''Causality and Kramers–Kronig relations for waveguides,'' *Opt. Exp.*, vol. 13, no. 24, pp. 9922–9934, Nov. 2005.

[16] D. Miller and P. L. Richards, ''Use of Kramers–Kronig relations to extract the conductivity of high-T_c superconductors from optical data,'' *Phys. Rev. B, Condens. Matter*, vol. 47, no. 18, pp. 12308–12311, May 1993.

[17] M. O'Donnell, E. T. Jaynes, and J. G. Miller, ''Kramers–Kronig relationship between ultrasonic attenuation and phase velocity,'' *J. Acoust. Soc. Amer.*, vol. 69, no. 3, pp. 696–701, Mar. 1981.

[18] E. C. Titchmarsh, *Introduction to the Theory of Fourier Integrals*, 2nd ed. London, U.K.: Oxford Univ. Press, 1948, pp. 128–129.

[19] D. M. Pozar, *Microwave Engineering*, 4th ed. New York, NY, USA: Wiley, 2011, pp. 172–174.

[20] A. A. Oliner, ''Historical perspectives on microwave field theory,'' *IEEE Trans. Microw. Theory Techn.*, vol. MTT-32, no. 9, pp. 1022–1045, Sep. 1984.

[21] A. Tip, ''Linear dispersive dielectrics as limits of Drude–Lorentz systems,'' *Phys. Rev. E, Stat. Phys. Plasmas Fluids Relat. Interdiscip. Top.*, vol. 69, p. 016610, Jan. 2004.

[22] B. Gralak and A. Tip, ''Macroscopic Maxwell's equations and negative index materials,'' *J. Math. Phys.*, vol. 51, no. 5, p. 052902, May 2010.

[23] *Novocontrol Technologies*. Accessed: Jan. 12, 2017. [Online]. Available: http://www.novocontrol.de

[24] *FCA—LATAM—Electric & Electronic Engineering*, Fiat Chrysler Automobiles-LATAM, Betim, Brazil, 2016.

ROBERTO BATISTA SARDENBERG received the bachelor's degree in physics in 2008 and the Ph.D. degree from the Universidade Federal de Minas Gerais, Belo Horizonte, Brazil, in 2015. He is currently a Teacher with the Faculdade de Engenharia de Minas Gerais.

His research interests include the electrical characterization, modeling and simulation of electrical devices, biosensors, and electrochemical cells.

He is also involved in fundamental aspects of the Impedance Spectroscopy measurement technique, and the characterization of nanostructured materials through the use of this technique.

JOSÉ M. A. FIGUEIREDO received the Ph.D. degree in physics from the Universidade Federal de Minas Gerais, Brazil, in 1993. In 1998, he was a Visiting Researcher with the Physics Department, City College of New York. He is currently an Associate Professor with the Institute of Exact Sciences, Physics Department, Universidade Federal de Minas Gerais. His main research interests include complex systems, foundations of quantum mechanics and basic research on radio frequency, and impedance measurements.